Softly Constrained Denoisers for Diffusion Models

Victor M. Yeom-Song[1,2] **Severi Rissanen**[1,2]
Arno Solin[1,2] **Samuel Kaski**[1,2,3] **Mingfei Sun**[3]
[1]ELLIS Institute Finland [2]Aalto University [3]University of Manchester
{victor.yeomsong,severi.rissanen,arno.solin,samuel.kaski}@aalto.fi
mingfei.sun@manchester.ac.uk

Abstract

Diffusion models struggle to produce samples that respect constraints, a common requirement in scientific applications. Recent approaches have introduced regularization terms in the loss or guidance methods during sampling to enforce such constraints, but they bias the generative model away from the true data distribution. This is a problem, especially when the constraint is misspecified, a common issue when formulating constraints on scientific data. In this paper, instead of changing the loss or the sampling loop, we integrate a guidance-inspired adjustment into the denoiser itself, giving it a soft inductive bias towards constraint-compliant samples. We show that these *softly constrained denoisers* exploit constraint knowledge to improve compliance over standard denoisers, and maintain enough flexibility to deviate from it when there is misspecification with observed data.

1 Introduction

Generating realistic data that satisfies specific constraints is a fundamental requirement across numerous applications in scientific discovery, ranging from finding solutions for ODEs [5] to designing proteins with certain properties [19]. Deep learning techniques have been proposed to solve many of these problems, with varying degrees of success [9, 8, 46, 37]. One of the most popular frameworks used in differential equation-based applications is that of *Physics-Informed Neural Networks* [44], where the differential equation residual is used to "inform" the training objective of the neural network, typically through the addition of a residual that quantifies how much the neural network solution deviates from "obeying" the differential equation.

A common pain point in these applications of deep learning has been that neural networks struggle to balance the competing objectives of maintaining data fidelity while satisfying the constraints. Without careful fine-tuning, these methods tend to get stuck on poor local minima that do not reflect the true data distribution [32] or simply result in solutions that do not fulfill the constraints [26]. This is particularly problematic when the training data deviates from the mathematical model used to formulate the constraints [16, 64].

Diffusion models [20, 53] have garnered attention due to their high sample quality, with recent methods exploring their use in inverse problems [11, 51, 4] and solving physical differential equations [25, 2]. Some of these diffusion-based approaches have explored the use of pre-trained unconditional models, i.e., models that learn the Stein score, to learn a "guidance" adjustment term on some constraint to guide the diffusion process towards data points that satisfy it [11, 51]. Another branch of research has explored the use of optimization during training the model using a regularizer while training the model [25, 2]. In the former approach, approximations in the inference-time adjustments cause bias in the modeled distribution, and the end result may not improve constraint satisfaction significantly over a standard diffusion model, as they are based on various simplifying approximations. The latter approaches can make optimization more difficult and bias the generative distribution away from the data [64, 1], as illustrated in Fig. 1.

Published in the AI for Science workshop (NeurIPS 2025).

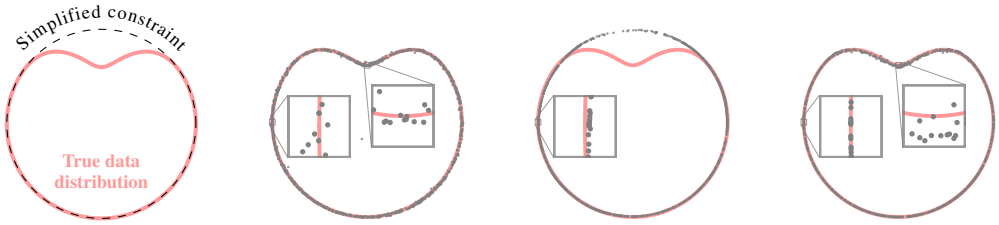

(a) Problem setup (b) Vanilla diffusion (c) PIDM (baseline) (d) SCD (ours)

Figure 1: Using a regularizer-based Physics Informed Diffusion Model to enforce the misspecified constraint makes it hard to capture the true data distribution compared to an unconstrained vanilla diffusion. Our method makes the best of the constraint information and vanilla diffusion properties, where it satisfies the partial constraint when it is useful, while maintaining enough flexibility to capture the true geometry.

In this paper, we present *Softly Constrained Denoisers* (SCD) for diffusion models. Inspired by guidance literature [11, 51, 52], we propose a method to endow diffusion model denoisers with constraint knowledge by incorporating a differentiable residual function into the forward pass of the network. Using this approach, we considerably improve constraint satisfaction compared to vanilla diffusion models and approximate guidance-based methods, while keeping a low amount of distributional bias. We present our main ideas and results on an illustrative example and a representative PDE problem.

The contributions of this paper are summarized as follows.

- We propose a method to transform any denoiser architecture to a "softly constrained denoiser" that has an inductive bias towards generating samples that satisfy the constraint. The constraints are embedded in the neural net architecture through the addition of a guidance-like adjustment term that is optimized end-to-end. This adds little computational overhead and preserves the asymptotic data fitting guarantees of standard diffusion models.
- We prove that previous regularizer-based methods cause bias that breaks the standard distribution-modeling guarantees of diffusion models. We show empirically that these methods perform especially poorly with constraint misspecification in representative differential equation problems. In contrast, our method retains all the distribution-modeling guarantees of standard diffusion due to only changing the neural net architecture, and can can extract useful knowledge from the constraint while keeping enough flexibility to deviate from the constraint if the data is not described by it (see Fig. 1 for an example).
- We demonstrate strong empirical results of the effectiveness of our approach through experiments on both illustrative problems and a PDE benchmark, showing that softly constrained denoisers achieve superior constraint satisfaction compared to existing methods, while maintaining sample quality and robustness under constraint misspecification.

2 Background

Diffusion models generate samples from a data distribution $p(\boldsymbol{x}_0)$ by learning how to denoise samples from a forward *noising* process [50, 20, 53, 27], which is generally assumed to be of the form:

$$p(\boldsymbol{x}_t) = \int \mathcal{N}\left(\boldsymbol{x}_t; \boldsymbol{x}_0, \sigma(t)^2\mathbf{I}\right) p(\boldsymbol{x}_0)\, \mathrm{d}\boldsymbol{x}_0. \tag{1}$$

In simpler terms, clean samples $\boldsymbol{x}_0$ from the data distribution $p(\boldsymbol{x}_0) = p_{\text{data}}(\boldsymbol{x}_0)$ are corrupted by a Gaussian process $\mathcal{N}(\mathbf{0}, \sigma(t)^2\mathbf{I})$ at time t. The corresponding reverse *denoising* process can be formulated as a probability flow ODE [27]:

$$\mathrm{d}\boldsymbol{x}_t = -\dot{\sigma}(t)\sigma(t)\nabla_{\boldsymbol{x}} \log p(\boldsymbol{x}_t)\, \mathrm{d}t. \tag{2}$$

Starting with a sample from an isotropic Gaussian $\mathcal{N}(\boldsymbol{x}_t; \boldsymbol{x}_0, \sigma_{\text{max}}^2\mathbf{I})$ and integrating the ODE backwards in time, it is possible to recover a sample from the original data distribution $\boldsymbol{x} \sim p(\boldsymbol{x}_0)$, as long as the score is learned accurately and σ_{max} is large enough [53]. To get $\nabla_{\boldsymbol{x}_t} \log p(\boldsymbol{x}_t)$, we first

learn a denoiser conditional on the noise level t:

$$\mathcal{L}(\theta) = \mathbb{E}_{t\sim p(t), \boldsymbol{x}_0 \sim p_{\text{data}}, \boldsymbol{x}_t \sim p(\boldsymbol{x}_t \mid \boldsymbol{x}_0)} \left[w(t) \| D_\theta(\boldsymbol{x}_t, t) - \boldsymbol{x}_0 \|^2 \right], \tag{3}$$

where $w(t)$ and $p(t)$ define the weighting and sampling frequency of noise levels during training, and D_θ is diffusion model's denoiser with parameters θ. At convergence, $D_\theta(\boldsymbol{x}_t, t) \approx \mathbb{E}[\boldsymbol{x}_0 \mid \boldsymbol{x}_t]$. Combined with Tweedie's formula $\mathbb{E}[\boldsymbol{x}_0 \mid \boldsymbol{x}_t] = \boldsymbol{x}_t + \sigma(t)^2 \nabla_{\boldsymbol{x}_t} \log p(\boldsymbol{x}_t)$, this ensures that we can recover an approximation of the score $\nabla_{\boldsymbol{x}_t} \log p(\boldsymbol{x}_t)$ with $s_\theta(\boldsymbol{x}_t) = \frac{D_\theta(\boldsymbol{x}_t) - \boldsymbol{x}_t}{\sigma(t)^2}$. Accordingly, the loss in Eq. (3) is also called the *denoising score matching* loss [57, 53] in the diffusion literature.

Distributional Bias The core problem in generative modeling is to learn a surrogate distribution $p_\theta(\boldsymbol{x})$ parameterized by θ to approximate a data distribution $p_{\text{data}}(\boldsymbol{x})$ [55]. We call a generative framework *biased* if $p_\theta(\boldsymbol{x})$ does not converge to $p_{\text{data}}(\boldsymbol{x})$ under optimal conditions, i.e., after finding the global optimum of the loss with infinite data, the sampling procedure does not result in samples from $p_{\text{data}}(\boldsymbol{x})$. Importantly, the diffusion model training and sampling in Eq. (3) and Eq. (2) is unbiased in this sense and can thus approximate any data distribution.

Guided Generation Assume we have a *constraint function* $c(\boldsymbol{x})$ where the constraint is satisfied when $c(\boldsymbol{x}) = 1$ and not satisfied when $c(\boldsymbol{x}) = 0$. Given a diffusion model with output distribution $p(\boldsymbol{x}_0)$, we can turn it into a constrained model with distribution $p(\boldsymbol{x}_0)c(\boldsymbol{x}_0)$ by adjusting the score as follows [51, 11]:

$$s_{\text{adjusted}}(\boldsymbol{x}_t) = \nabla_{\boldsymbol{x}_t} \log p(\boldsymbol{x}_t) + \nabla_{\boldsymbol{x}_t} \log \int c(\boldsymbol{x}_0) p(\boldsymbol{x}_0 \mid \boldsymbol{x}_t) \, \mathrm{d}\boldsymbol{x}_0. \tag{4}$$

Many methods have been proposed in the diffusion guidance literature for approximating the second term on the right hand side [21, 51, 11, 52, 47], which generally can be summarized in choosing an approximation for the distribution $p(\boldsymbol{x}_0 \mid \boldsymbol{x}_t)$ and an approximation scheme for the integral, e.g. Monte Carlo integration. The idea is to do these approximations at inference time without any changes to the weights of the trained model. While inference-time adjustments are convenient, any error in the approximation results in bias in the output distribution of the diffusion model, and constraint satisfaction is only approximate.

Regularization Another approach to constrain the generative space of a model is to use *regularizers* on the training objective. Popularized by *Physics Informed Neural Networks* [44], the general idea is to have an optimization target that is expanded with a differentiable constraint, typically a residual $\mathcal{R} : \mathbb{R}^d \to \mathbb{R}$ related to a differential equation for a physical system, as follows:

$$\mathcal{L}_{\text{target}}(\theta) = \mathcal{L}(\theta) + \lambda \|\mathcal{R}(\theta)\|, \tag{5}$$

where $\lambda \geq 0$ is a hyperparameter that defines how much weight to give to the constraint compliance, the residual $\mathcal{R}$ is used to evaluate the output of a neural network with parameters θ and $\|\cdot\|$ is some scalar norm of choice, e.g., L_p. Although intuitively the target distribution of the learning task should naturally learn to minimize this residual, these PDE-based regularizers can make the loss landscape hard to optimize [32, 45]. Further, the optimum of Eq. (5) forfeits the property that $D_\theta(\boldsymbol{x}_t, t) \approx \mathbb{E}[\boldsymbol{x}_0 \mid \boldsymbol{x}_t]$ at convergence and the connection between the denoiser and $\nabla_{\boldsymbol{x}_t} \log p(\boldsymbol{x}_t)$ is lost (see Proposition 3.1). Thus, the addition of these targets in the loss function causes bias in the generative distribution [2, 1].

Constraint Misspecification In science, we build simplified mathematical models around complex phenomena and systems to allow us to study and make use of them. However, since these models are inherently approximations to real phenomena, they are bound to have varying degrees of *misspecification*. We say a constraint is misspecified if it rules out anything that belongs to the true data distribution. Formally, for a constraint $c(\boldsymbol{x}) \in \{0, 1\}$ where $\{\boldsymbol{x} : c(\boldsymbol{x}) = 1\}$ is the constraint-satisfying set, the constraint is misspecified if for any $\boldsymbol{x}$, $p_{\text{data}}(\boldsymbol{x})c(\boldsymbol{x}) \neq p_{\text{data}}(\boldsymbol{x})$.

3 Methods

A key limitation of guidance and regularization methods is that they forfeit the theoretical guarantees provided by training a denoiser with Eq. (3) and directly using it for sampling through Eq. (2). One aspect not determined by the diffusion model's mathematics, however, is the neural architecture of the denoiser $D_\theta(\boldsymbol{x}_t, t)$. In principle, this can be parameterized freely. This flexibility motivates us to embed the constraint function $c(\boldsymbol{x})$ directly into $D_\theta(\boldsymbol{x}_t, t)$, imparting an inductive bias

towards constraint satisfaction while still allowing deviations when the constraint does not faithfully represent the training data. In this section, we present a principled way of constructing such denoiser parameterizations, building on connections to the guidance literature and Eq. (4).

Class of Constraints In this paper, we consider constraints that are possible to write in a form $\mathcal{R}(\boldsymbol{x}) = 0$, where $\mathcal{R}$ is some function. Thus, $c(\boldsymbol{x}) = 1$ for all $\boldsymbol{x}$ in $\{\boldsymbol{x} : \mathcal{R}(\boldsymbol{x}) = 0\}$ and 0 elsewhere. This could, for instance, be a finite difference based residual formed from a PDE, or a circle in 2D, where $\mathcal{R}(\boldsymbol{x}) = x_1^2 + x_2^2 - 1$. We further assume $\mathcal{R}$ to be continuously differentiable in the input $\boldsymbol{x}$, such that we can calculate gradients $\nabla_{\boldsymbol{x}}\mathcal{R}(\boldsymbol{x})$. We then define a *relaxed constraint function* $l_c(\boldsymbol{x}) = \exp(-\|\mathcal{R}(\cdot)\|)$ for some choice of norm $\|\cdot\|$, similar to the recipe prescribed by Song et al. [52], connecting our method with the guidance literature. Importantly, the norm and more broadly the design of $l_c(\boldsymbol{x})$ is a design choice for our method, and we could design it in any way that provides information about the constraint to the denoiser architecture.

Guidance Approximation Following common ideas in the guidance literature, we first propose a practical approximation to Eq. (4).This leads to a formula that nudges the denoiser towards satisfying the constraint by using the gradient of a (relaxed) constraint function $\nabla_{\boldsymbol{x}_0} l_c(\boldsymbol{x}_0)$. We then use this approximate form as an inspiration for a denoiser parameterization that learns to calibrate this gradient-based nudge, freeing the base neural network from having to output values that are perfectly aligned with the constraints.

First we choose an approximation to $p(\boldsymbol{x}_0 \mid \boldsymbol{x}_t)$ in Eq. (4). A common choice is $p(\boldsymbol{x}_0 \mid \boldsymbol{x}_t) = \mathcal{N}(D_\theta(\boldsymbol{x}_t, t), \Sigma_{0|t}^2 \mathbf{I})$, where $\Sigma_{0|t}^2$ is a hyperparameter [21, 51, 11, 4, 41, 47]. Similarly to Chung et al. [11], we choose $\sigma_{0|t}^2 = 0$. Thus, $p(\boldsymbol{x}_0 \mid \boldsymbol{x}_t)$ turns into a Dirac delta on $D_\theta(\boldsymbol{x}_t, t)$ and taking the integral in Eq. (4) with this choice produces the following:

$$s_\theta^{\text{guided}}(\boldsymbol{x}_t) \approx \frac{D_\theta(\boldsymbol{x}_t, t) - \boldsymbol{x}_t}{\sigma_t^2} + \nabla_{\boldsymbol{x}_t} \log l_c\left(D_\theta(\boldsymbol{x}_t, t)\right). \tag{6}$$

This expression results in a vector-Jacobian product through the denoiser, which can result in considerable computational overhead:

$$\nabla_{\boldsymbol{x}_t} \log l_c\left(D_\theta(\boldsymbol{x}_t, t)\right)^\top = \nabla_{D_\theta} \log l_c\left(D_\theta(\boldsymbol{x}_t, t)\right)^\top \nabla_{\boldsymbol{x}_t} D_\theta(\boldsymbol{x}_t, t). \tag{7}$$

To obtain a more efficient approximation, we recall that the Jacobian is connected to the denoising covariance through $\nabla_{\boldsymbol{x}_t} D_\theta(\boldsymbol{x}_t, t) = \frac{\text{Cov}[\boldsymbol{x}_0 \mid \boldsymbol{x}_t]}{\sigma(t)^2}$ [4]. Analogous to our earlier treatment of $p(\boldsymbol{x}_0 \mid \boldsymbol{x}_t)$, we approximate the conditional covariance as $\text{Cov}[\boldsymbol{x}_0 \mid \boldsymbol{x}_t] \approx \boldsymbol{\Lambda}_t$, where $\boldsymbol{\Lambda}_t$ is some diagonal matrix. Altogether, this yields the following denoiser correction:

$$D_{\theta,\text{guided}}(\boldsymbol{x}_t, t) = D_\theta(\boldsymbol{x}_t, t) + \boldsymbol{\Lambda}_t \sigma(t)^2 \nabla_{\boldsymbol{D}_\theta} \log l_c(D_\theta(\boldsymbol{x}_t, t)). \tag{8}$$

Softly Constrained Denoiser The key idea in our paper is as follows: since Eq. (8) tends to generate samples that satisfy the constraint for a suitably chosen $\boldsymbol{\Lambda}_t$, we can form a denoiser parameterization that uses the same structure for easier constraint compliance through a learned $\boldsymbol{\Lambda}_t$ term

$$D_\theta(\boldsymbol{x}_t, t) = D_\theta^{\text{orig}}(\boldsymbol{x}_t, t) + \boldsymbol{\gamma}_\theta(\boldsymbol{x}_t, t)\sigma(t)^2 \nabla_{\boldsymbol{D}_\theta^{\text{orig}}} \log l_c(D_\theta^{\text{orig}}(\boldsymbol{x}_t, t)), \tag{9}$$

where $D_\theta^{\text{orig}}(\boldsymbol{x}_t, t)$ is the original denoiser output and $\boldsymbol{\gamma}_\theta(\boldsymbol{x}_t, t)$ is a learnable scaling factor that can be parameterized by the same base neural network as $D_\theta^{\text{orig}}(\boldsymbol{x}_t, t)$, or by a separate network. The model can then be trained using the standard denoising score matching loss in Eq. (3). Crucially, the correction term in Eq. (9) only evaluates the gradient of the constraint l_c until D_θ, avoiding the costly calculation of a vector-Jacobian product in the forward pass. While we adopt this particular approximation, many alternative (and potentially more sophisticated) formulations of the guidance formula are possible. Each such choice would naturally define a corresponding softly constrained denoiser, making our approach a general recipe for deriving new variants. In our experiments, we focus on Eq. (9) and leave more sophisticated parameterizations for future work. We show the training algorithm explicitly in Algorithm 1 and visualize the new denoiser architecture in Fig. 2.

3.1 Analysis of Regularization Bias and ELBO Degradation

In this section, we formally analyze the impact of introducing a regularization term to the training objective, as proposed in PIDM [2]. We demonstrate that while this regularization enforces constraint

Algorithm 1 Loss for SCD

Require: Data $p_{data}(\boldsymbol{x})$, constraint $l_c(\boldsymbol{x})$, noise $\sigma(t)$, weights $w(t)$, noise $p(t)$

Init $\boldsymbol{\theta}$; Sample $\boldsymbol{x}_0, t, \boldsymbol{\epsilon}$
$\boldsymbol{x}_t \leftarrow \boldsymbol{x}_0 + \sigma(t)\boldsymbol{\epsilon}$
Compute SCD Output $\hat{\boldsymbol{x}}_{\boldsymbol{\theta}}$:
$\hat{\boldsymbol{x}}_{base} \leftarrow D_{\boldsymbol{\theta}}^{orig}(\boldsymbol{x}_t, t)$
$g \leftarrow \nabla_{\boldsymbol{x}} \log l_c(\hat{\boldsymbol{x}}_{base})$
$\hat{\lambda} \leftarrow \gamma_{\boldsymbol{\theta}}(\boldsymbol{x}_t, t)\sigma(t)^2$
$\hat{\boldsymbol{x}}_{\boldsymbol{\theta}} \leftarrow \hat{\boldsymbol{x}}_{base} + \hat{\lambda} \cdot g$
Output Loss:
$\mathcal{L} \leftarrow w(t)\|\hat{\boldsymbol{x}}_{\boldsymbol{\theta}}(\boldsymbol{x}_t, t) - \boldsymbol{x}_0\|^2$

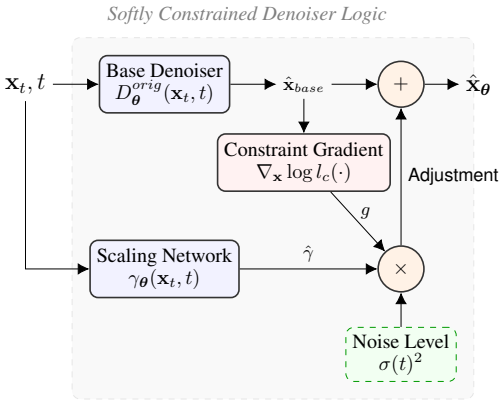

Figure 2: Architecture of SCD.

satisfaction, it biases the denoiser away from the true conditional expectation and also necessarily degrades the variational lower bound (ELBO) of the diffusion model [20, 31].

Consider the regularized objective function for a specific noise level t (ignoring the weighting term $w(t)$ for brevity):

$$\mathcal{L}_{\text{reg}}(\theta) = \mathbb{E}_{x_0, x_t}\left[\|D_\theta(x_t, t) - x_0\|^2\right] + \lambda\|\mathcal{R}(D_\theta(x_t, t))\|^2, \tag{10}$$

where $\lambda > 0$ is the regularization weight and $\mathcal{R}$ is the constraint residual.

Proposition 3.1. *Let $D^*_{reg}(x_t, t)$ be the denoiser that minimizes the regularized objective $\mathcal{L}_{reg}$. The optimal denoiser output is shifted from the true conditional mean of the data distribution by a term proportional to the gradient of the residual. Specifically:*

$$D^*_{reg}(x_t, t) = \mathbb{E}[x_0|x_t] - \lambda\left[\nabla_y \mathcal{R}(y)\right]^\top \mathcal{R}(y)\Big|_{y=D^*_{reg}}, \tag{11}$$

where we assume a scalar constraint residual for simplicity, or $\mathcal{R}$ represents the norm function directly. Since $\mathbb{E}[x_0 \mid x_t]$ does not generally satisfy the constraint, and the residual or its gradient are zero only when the constraint is satisfied, the optimal denoiser output is shifted. The asymptotic distributional guarantees of diffusion models are thus lost since there is no connection between the optimal denoiser and the score function $\nabla_{\boldsymbol{x}_t} \log p(\boldsymbol{x}_t)$.

Proposition 3.2. *The use of the regularized denoiser D^*_{reg} strictly increases the Evidence Lower Bound (ELBO) loss component compared to the vanilla denoiser $D^*_{vanilla}$. That is, the model's approximation of the data likelihood deteriorates.*

See Appendix A for the proofs. Note that the PIDM paper [2] also considered regularising based on a DDIM integration output, but their best results were obtained by regularising the $D_\theta(x_t, t)$ directly.

4 Related Work

Here we cover related work most relevant to our approach. See Appendix B for more related work on enforcing constraints through modifications to the sampling process.

Diffusion Models Applied to PDEs Jacobsen et al. [25] propose conditional PDE generation using a Controlnet-like conditioning structure [62] and an inference-time adjustment where the final samples are optimized to have a small PDE residual. Bastek et al. [2] present Physics-Informed Diffusion Models (PIDM), a framework to train DDPM-based diffusion models with a PDE residual as a regularizer term to minimize along the loss function. Several works utilize DPS-like guidance [11] for PDE data assimilation, targeting noisy measurements [49], constraint satisfaction [24], or infinite-dimensional Banach spaces [61]. Similarly, Cheng et al. [7] employ projection-based sampling [63]. Unlike these, our method avoids approximate inference-time guidance. Furthermore, our parameterization is orthogonal to recent architecture-focused works on neural operators [22, 40] or GNNs [56], as it remains compatible with any base architecture.

Injecting Measurement Structure for Training Inverse Problem Solvers Mathematically, the closest work is the likelihood-informed Doob's h-transform by Denker et al. [14], who finetune

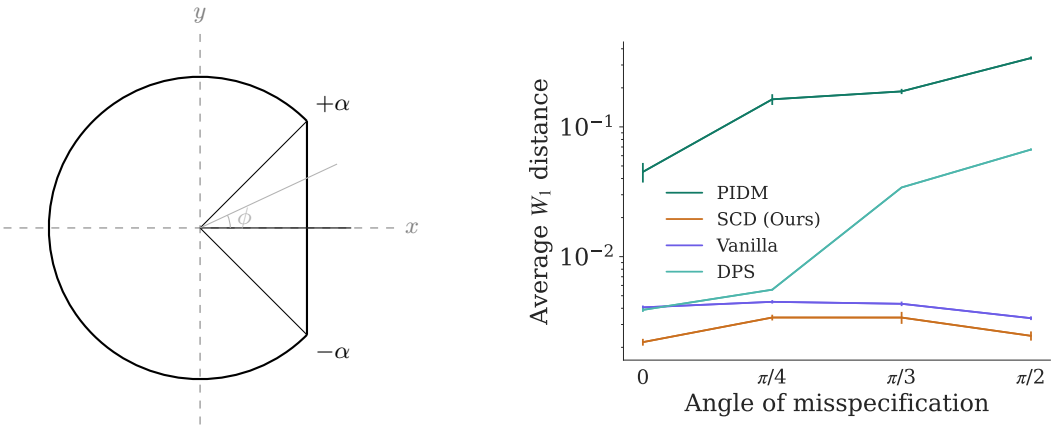

Figure 3: (a) "Chop" misspecification for our experiments. For all points with angles $-\alpha < \phi < \alpha$ the x coordinate is projected to $x = \cos\alpha$. (b) Average Wasserstein-1 distances on the circles examples with varying degrees of misspecification on "Chop". Vanilla and SCD keep steady values of W_1 distance which indicates their flexibility to learn the true data distribution, whereas PIDM consistently increases with higher levels of misspecification. Means drawn with two standard deviations.

adapters using observation gradients $\nabla_{\boldsymbol{x}_0} p(\boldsymbol{y} \mid \boldsymbol{x}_0)$, similar to our constraint-informed parameterization using $\nabla_{\boldsymbol{x}_0} l_c(\boldsymbol{x}_0)$. However, our motivation and methodology differ: they use likelihoods $p(\boldsymbol{y} \mid \boldsymbol{x}_0)$ for Bayesian inference from noisy observations, whereas we *define* $l_c(\boldsymbol{x}_0)$ to restrict generation to a constrained subset. Their goal is an alternative to inference-time adjustment, while we seek to alleviate distributional biases and constraint misspecification. Furthermore, we train from scratch, whereas they finetune adapters on larger models. Finally, Liu et al. [34], Chung et al. [12] propose embedding structure via bridge processes that interpolate between condition and target; this is inapplicable to our setting, as we do not target a translation problem.

Distributional Constraints Khalafi et al. [29] formulate a distributional constrained generation task with the constraint that the generative distribution should have a KL divergence below a threshold to a set of auxiliary distributions q^i. Khalafi et al. [30] extend the idea to compositional generation.

Soft Inductive Biases Finzi et al. [16] propose using "dual path" layers to build a neural network, where one path uses a hard-constrained layer, e.g. a rotationally equivariant layer, and the other uses a more "relaxed" layer. By assigning a lower prior probability to the relaxed path, a soft inductive bias towards solutions that satisfy the constraint is imposed, without restricting the possible hypothesis space for the neural network.

5 Experiments

We first showcase and analyze our method on an illustrative set of toy examples in Section 5.1. In Section 5.2, we evaluate our method on the Darcy flow PDE data set, a commonly used benchmark in the diffusion scientific constrained generation literature [25, 2]. Additional results on the Helmholtz Equation, with comparisons with FunDPS [61], are accessible in Appendix D. For all experiments, γ_θ was implemented as a small 2-layer MLP that takes $D_\theta(\boldsymbol{x}_t)$ and t as input and outputs a scalar. Details are available in Appendix F. We also use a modified version of the loss function by Karras et al. [27]: in our experiments we observed that the models had issues with refining the fine-grained details at the lower noise levels, and modifying the distribution from which the noise levels are sampled significantly improved the results across all models. The details of the modification are available in Appendix F.1

5.1 Illustrative Examples

We explore our method in new variants of the toy data set introduced by Bastek et al. [2], introducing new misspecification modalities. The data itself is simply points sampled from the unit circle centered at the origin, and we train a diffusion model to learn to produce samples on the circle. Given a sample $(x, y) \in \mathbb{R}^2$, we define a residual function for this setting with the following equation:

$$\mathcal{R}_{\text{circle}}(x, y) = \left(\sqrt{x^2 + y^2} - 1\right)^2. \tag{12}$$

Table 1: Measured (**best**) Wasserstein-1 distances from the true data distribution with each method. All the values are presented as the mean with two standard deviations across 100 estimates with 1000 samples taken from each method. Lower is better. All values are multiplied by 10^{-3}.

Method	**Unit circle**	**Dent**	**Chop** ($\alpha = \frac{\pi}{2}$)
Vanilla	3.91 ± 0.18	7.53 ± 0.46	3.34 ± 0.11
PIDM	4.04 ± 0.20	6.65 ± 1.44	33.75 ± 3.37
SCD (ours)	$\mathbf{2.16 \pm 0.15}$	$\mathbf{5.6 \pm 0.44}$	$\mathbf{2.42 \pm 0.16}$

The architecture and training details are shown in Appendix F.2. We use $r_c = \exp(-\mathcal{R}_{\text{circle}}(x, y))$ as our constraint term for these experiments. We then evaluate the performance of vanilla diffusion, regularizer based diffusion (PIDM) and our method on a few examples of misspecification. Specifically, we use Eq. (12) with PIDM and our method on variations of the circle, namely a circle with a "dent" on top and a circle that is "chopped" after a particular x coordinate.

For "Dent", we use a circle with a polynomial interpolation at the top half. This produces the shape seen in Fig. 1, the details on the interpolation are available in Appendix F.2. For "Chop", as illustrated in Fig. 3, we define an angle threshold $-\alpha < \phi < \alpha$ for which all points on the circle with angle ϕ have their x coordinate projected to $\cos \alpha$.

The results of using vanilla diffusion, PIDM, and our method on the standard circle and the two described misspecifications are summarized in Table 1. We can see that in the case of the unit circle, all methods achieve relatively similar W_1 distances, indicating that all are capable of capturing the underlying geometry. For "Dent", we see that PIDM starts to have higher values, and we can see from Fig. 1 that this is because training with PIDM makes the model incapable of putting samples on the dent. This issue is most prominent with "Chop", where the W_1 distance with PIDM is almost an order of magnitude higher than the other two methods: this is because it does not put any mass on the projected line, it only learns the samples on the arc along the circle.

To measure the effect of varying the misspecifications on the toy data, we vary the angle for "Chop" and note the change on the W_1 distance. This is seen on Fig. 3. Both vanilla diffusion and our method stay relatively steady for all different α, while PIDM sees a steady increase with higher degrees of misspecification. Note the W_1 distance for PIDM is worse than vanilla diffusion even when the constraint is correctly specified at $\alpha = 0$, potentially due to the distribution being biased *along the circle* even if the constraint is satisfied. Similar issues were visually noticed in [2] when using a high weight on the regularization term.

5.2 Darcy Flow

The task is to learn how to produce samples of a permeability field $K(x, y)$ and a pressure field $p(x, y)$ in two dimensions $(x, y) \in \mathbb{R}^2$ that satisfy the following differential equation:

$$\mathcal{R}_{\text{Darcy}}(K, p) = \nabla \cdot (K \nabla p) + f = 0, \tag{13}$$

where f is the measurement of the flow of some fluid through a porous medium, and corresponds to the divergence of the vector field defined by $K\nabla p$, or the *net* amount of fluid entering and exiting a given point. For a brief treatment on the topic, see Appendix C.

This differential equation doubles as a residual function we can use to verify our generated solutions. For the experiments, the differential terms are estimated through finite differences using the same stencils used by Bastek et al. [2], meaning K and p are sampled as matrices in $\mathbb{R}^{n \times n}$. We use this implementation to define our constraint adjustment $r_c = \exp(-|\mathcal{R}_{\text{Darcy}}(K, p)|)$, where K and p are the denoiser outputs. To tackle this problem, we use a diffusion model with a UNet backbone developed by Karras et al. [28], and use a discretization of K and p in $\mathbb{R}^{64 \times 64}$. The architecture, training details and runtimes are available in Appendix F.3. We highlight the small relative overhead in runtime between our method and a vanilla score matching implementation.

Distributional Fidelity, Misspecification and Residuals Darcy Flow is a mathematical model particularly used to infer properties of a material in a real physical system. As such, using this model can be prone to different sources of error, ranging from measurement error (e.g., miscalibrated tools, noisy environments) to using it on a system with critical flow, where the fluid is in a state between laminar and turbulent flow. In this section, we present experiments on a simple case where the measured flow is on a wrong scale (an example of miscalibration).

Table 2: Measured (**best**, second best) residual values and validation set NLL of the different methods across different levels of source and sink misspecification. Our method shows good performance across all misspecification levels. Residual values presented are mean absolute residuals across 1000 samples with two standard deviations and NLL values are on the complete validation set, reported in bits/dim. Vanilla does not use the constraint knowledge, so we treat it the same for all levels as a baseline. Lower is better.

		Original	*increasing misspecificication* →		
Metric	**Method**	$f_{\max} = 10$	$f_{\max} = 20$	$f_{\max} = 30$	$f_{\max} = 40$
Residual	Vanilla	0.157 ± 0.071	0.157 ± 0.071	0.157 ± 0.071	0.157 ± 0.071
	Guided Vanilla	0.141 ± 0.063	0.139 ± 0.067	0.140 ± 0.065	0.139 ± 0.066
	PIDM	$\mathbf{0.025 \pm 0.010}$	$\mathbf{0.332 \pm 0.007}$	0.647 ± 0.007	0.963 ± 0.009
	SCD (ours)	0.113 ± 0.048	0.106 ± 0.049	$\mathbf{0.114 \pm 0.059}$	$\mathbf{0.118 \pm 0.051}$
NLL	Vanilla	$\mathbf{-10.5}$	$\mathbf{-10.5}$	$\mathbf{-10.5}$	$\mathbf{-10.5}$
	Guided Vanilla	-10.3	-10.3	-10.3	-10.3
	PIDM	-3.7	-3.7	-3.6	-3.2
	SCD (ours)	-8.4	-6.9	-5.9	-5.8

To induce the misspecification, we test out different values for the measured flow f in the constraint, while keeping the original data. The results using vanilla, guided vanilla, PIDM and our method are shown in Table 2 reported with residual values and NLL. The vanilla diffusion with inference-time guidance is implemented using Eq. (6) following "Loss Guided Diffusion" by Song et al. [52], and the guidance scale used for the guided vanilla was tuned to a value of 0.03 based on the residual values with a grid search. Details on this guidance method can be seen in Appendix E. Qualitative visualizations and samples from our method are available in Appendix C.1. We highlight that PIDM is especially sensitive to the induced misspecifications, causing its residuals to go up considerably to the point that it performs worse than a baseline vanilla diffusion model. On the other hand, our model shows relative resilience to these changes. We hypothesize that it can still use the information in the area where the f-field is correctly specified as zero, while learning to adapt the gradient information used for the source and the sink. Using a guidance method with vanilla diffusion slightly improves the residuals but not by a significant margin, and the same behavior continues across different misspecification levels.

6 Discussion and Conclusion

In this work, we introduced the Softly Constrained Denoiser (SCD), a simple way to embed constraint knowledge directly into diffusion model denoisers. Unlike guidance-based methods that add constraints only at inference time or regularization-based methods that bias the training distribution, our approach provides a soft inductive bias that improves constraint satisfaction while retaining flexibility when constraints are misspecified. We demonstrated these benefits through illustrative examples (Section 5.1) and PDE benchmarks (Section 5.2), showing that SCD outperforms standard diffusion models and existing constraint-enforcing approaches when the constraint is partially misspecified. Our results suggest that SCD can serve as a drop-in upgrade for diffusion-based generative modeling in applications where constraints are desired.

Limitations and Future Work A limitation of our proposed method is that our denoiser form is, at the end of the day, an approximation to the score function for the tilted distribution $r_c(\boldsymbol{x}_0)p(\boldsymbol{x}_0)$. As such, the approximation may limit the usefulness of the inductive bias that it provides. Another limitation is that our model is not guaranteed to generate samples within a particular hard constraint, and if an application requires exact constraint satisfaction, further postprocessing of generated samples is necessary. Finally, even though the inductive bias provided by the denoiser parameterization does not necessarily inhibit the diffusion model from following the data distribution, the parameterization may push the model towards particular biases in practice. Further, in the presence of significant misspecification the new parameterization may cause noise relative to standard denoisers. Future work could explore deriving SCDs based on more advanced guidance approximations and applying them in various scientific application areas. Even better robustness to constraint specification could be achieved by introducing learnable parameters to $l_c(\boldsymbol{x})$ itself.

Acknowledgements

This work was supported by the Research Council of Finland (Flagship programme: Finnish Center for Artificial Intelligence FCAI and decision 359207), ELLIS Finland, EU Horizon 2020 (European Network of AI Excellence Centres ELISE, grant agreement 951847). VYS acknowledges funding from the Finland Fellowship awarded by Aalto University. SK acknowledges funding from the UKRI Turing AI World-Leading Researcher Fellowship (EP/W002973/1).. AS and SR acknowledge funding from the Research Council of Finland (grants: 339730 and 362408). MS acknowledges funding from AI Hub in Generative Models by Engineering & Physical Sciences Research Council (EPSRC) with Funding Body Ref: EP/Y028805/1. The authors acknowledge the research environment provided by ELLIS Institute Finland, and then CSC – IT Center for Science, Finland, and the Aalto Science-IT project for computational resources.

References

[1] Giacomo Baldan, Qiang Liu, Alberto Guardone, and Nils Thuerey. Flow Matching Meets PDEs: A Unified Framework for Physics-Constrained Generation, 2025. preprint: arXiv:2506.08604.

[2] Jan-Hendrik Bastek, WaiChing Sun, and Dennis Kochmann. Physics-informed diffusion models. In *International Conference on Learning Representations (ICLR)*, 2025.

[3] Heli Ben-Hamu, Omri Puny, Itai Gat, Brian Karrer, Uriel Singer, and Yaron Lipman. D-flow: Differentiating through flows for controlled generation. In *Forty-first International Conference on Machine Learning (ICML)*, 2024.

[4] Benjamin Boys, Mark Girolami, Jakiw Pidstrigach, Sebastian Reich, Alan Mosca, and Omer Deniz Akyildiz. Tweedie Moment Projected Diffusions for Inverse Problems. *Transactions on Machine Learning Research*, 2024.

[5] Ricky T. Q. Chen, Yulia Rubanova, Jesse Bettencourt, and David K Duvenaud. Neural ordinary differential equations. In *Advances in Neural Information Processing Systems (NeurIPS)*. Curran Associates, Inc., 2018.

[6] Ricky TQ Chen and Yaron Lipman. Flow matching on general geometries. In *International Conference on Learning Representations (ICLR)*, 2024.

[7] Chaoran Cheng, Boran Han, Danielle C Maddix, Abdul Fatir Ansari, Andrew Stuart, Michael W Mahoney, and Bernie Wang. Gradient-free generation for hard-constrained systems. In *The Thirteenth International Conference on Learning Representations*, 2025.

[8] Gyouho Cho, Mengqi Wang, Youngki Kim, Jaerock Kwon, and Wencong Su. A physics-informed machine learning approach for estimating lithium-ion battery temperature. *IEEE Access*, 10:88117–88126, 2022.

[9] Pi-Yueh Chuang and Lorena A. Barba. Experience report of physics-informed neural networks in fluid simulations: Pitfalls and frustration. In *SciPy*, 2022.

[10] Hyungjin Chung, Byeongsu Sim, Dohoon Ryu, and Jong Chul Ye. Improving diffusion models for inverse problems using manifold constraints. In *Advances in Neural Information Processing Systems 35 (NeurIPS)*, pages 25683–25696, 2022.

[11] Hyungjin Chung, Jeongsol Kim, Michael Thompson Mccann, Marc Louis Klasky, and Jong Chul Ye. Diffusion posterior sampling for general noisy inverse problems. In *International Conference on Learning Representations (ICLR)*, 2023.

[12] Hyungjin Chung, Jeongsol Kim, and Jong Chul Ye. Direct diffusion bridge using data consistency for inverse problems. In *Advances in Neural Information Processing Systems 36 (NeurIPS)*, pages 7158–7169, 2023.

[13] Valentin De Bortoli, Emile Mathieu, Michael Hutchinson, James Thornton, Yee Whye Teh, and Arnaud Doucet. Riemannian score-based generative modelling. In *Advances in Neural Information Processing Systems 35 (NeurIPS)*, pages 2406–2422, 2022.

[14] Alexander Denker, Francisco Vargas, Shreyas Padhy, Kieran Didi, Simon Mathis, Riccardo Barbano, Vincent Dutordoir, Emile Mathieu, Urszula Julia Komorowska, and Pietro Lio. DEFT: Efficient fine-tuning of diffusion models by learning the generalised h-transform. In *Advances in Neural Information Processing Systems 37 (NeurIPS)*, pages 19636–19682, 2024.

[15] Bradley Efron. Tweedie's formula and selection bias. *Journal of the American Statistical Association*, 106(496):1602–1614, 2011.

[16] Marc Finzi, Gregory Benton, and Andrew G Wilson. Residual pathway priors for soft equivariance constraints. In *Advances in Neural Information Processing Systems (NeurIPS)*, pages 30037–30049. Curran Associates, Inc., 2021.

[17] Nic Fishman, Leo Klarner, Valentin De Bortoli, Emile Mathieu, and Michael John Hutchinson. Diffusion models for constrained domains. *Transactions on Machine Learning Research*, 2023.

[18] Nic Fishman, Leo Klarner, Emile Mathieu, Michael Hutchinson, and Valentin De Bortoli. Metropolis sampling for constrained diffusion models. In *Advances in Neural Information Processing Systems 36 (NeurIPS)*, pages 62296–62331, 2023.

[19] Nate Gruver, Samuel Don Stanton, Nathan C. Frey, Tim G. J. Rudner, Isidro Hotzel, Julien Lafrance-Vanasse, Arvind Rajpal, Kyunghyun Cho, and Andrew Gordon Wilson. Protein design with guided discrete diffusion. In *Advances in Neural Information Processing Systems 36 (NeurIPS)*, 2023.

[20] Jonathan Ho, Ajay Jain, and Pieter Abbeel. Denoising diffusion probabilistic models. In *Advances in Neural Information Processing Systems (NeurIPS)*, pages 6840–6851. Curran Associates Inc., 2020.

[21] Jonathan Ho, Tim Salimans, Alexey Gritsenko, William Chan, Mohammad Norouzi, and David J Fleet. Video Diffusion Models. In *Advances in Neural Information Processing Systems 35 (NeurIPS)*, pages 8633–8646, 2022.

[22] Peiyan Hu, Rui Wang, Xiang Zheng, Tao Zhang, Haodong Feng, Ruiqi Feng, Long Wei, Yue Wang, Zhi-Ming Ma, and Tailin Wu. Wavelet diffusion neural operator. In *The Thirteenth International Conference on Learning Representations*, 2025.

[23] Chin-Wei Huang, Milad Aghajohari, Joey Bose, Prakash Panangaden, and Aaron C Courville. Riemannian diffusion models. In *Advances in Neural Information Processing Systems 35 (NeurIPS)*, pages 2750–2761, 2022.

[24] Jiahe Huang, Guandao Yang, Zichen Wang, and Jeong Joon Park. Diffusionpde: Generative pde-solving under partial observation. In *Advances in Neural Information Processing Systems 37 (NeurIPS)*, pages 130291–130323, 2024.

[25] Christian Jacobsen, Yilin Zhuang, and Karthik Duraisamy. CoCoGen: Physically consistent and conditioned score-based generative models for forward and inverse problems. *SIAM Journal on Scientific Computing*, 47(2):C399–C425, 2025. doi: 10.1137/24M1636071.

[26] Petr Karnakov, Sergey Litvinov, and Petros Koumoutsakos. Solving inverse problems in physics by optimizing a discrete loss: Fast and accurate learning without neural networks. *PNAS Nexus*, 3(1):pgae005, January 2024.

[27] Tero Karras, Miika Aittala, Timo Aila, and Samuli Laine. Elucidating the design space of diffusion based generative models. In *Advances in Neural Information Processing Systems (NeurIPS)*, pages 26565–26577. Curran Associates, Inc., 2022.

[28] Tero Karras, Miika Aittala, Jaakko Lehtinen, Janne Hellsten, Timo Aila, and Samuli Laine. Analyzing and Improving the Training Dynamics of Diffusion Models. *2024 IEEE/CVF Conference on Computer Vision and Pattern Recognition (CVPR)*, pages 24174–24184, 2023.

[29] Shervin Khalafi, Dongsheng Ding, and Alejandro Ribeiro. Constrained diffusion models via dual training. In *Advances in Neural Information Processing Systems 37 (NeurIPS)*, pages 26543–26576, 2024.

[30] Shervin Khalafi, Ignacio Hounie, Dongsheng Ding, and Alejandro Ribeiro. Composition and alignment of diffusion models using constrained learning. In *2nd Workshop on Models of Human Feedback for AI Alignment*, 2025.

[31] Diederik Kingma, Tim Salimans, Ben Poole, and Jonathan Ho. Variational diffusion models. *Advances in neural information processing systems*, 34:21696–21707, 2021.

[32] Aditi Krishnapriyan, Amir Gholami, Shandian Zhe, Robert Kirby, and Michael W Mahoney. Characterizing possible failure modes in physics-informed neural networks. In *Advances in Neural Information Processing Systems (NeurIPS)*, pages 26548–26560. Curran Associates, Inc., 2021.

[33] Guan-Horng Liu, Tianrong Chen, Evangelos Theodorou, and Molei Tao. Mirror diffusion models for constrained and watermarked generation. In *Advances in Neural Information Processing Systems 36 (NeurIPS)*, pages 42898–42917, 2023.

[34] Guan-Horng Liu, Arash Vahdat, De-An Huang, Evangelos Theodorou, Weili Nie, and Anima Anandkumar. I^2sb: Image-to-image Schrödinger bridge. In *International Conference on Machine Learning (ICML)*, pages 22042–22062. PMLR, 2023.

[35] Aaron Lou and Stefano Ermon. Reflected diffusion models. In *International Conference on Machine Learning*, pages 22675–22701. PMLR, 2023.

[36] Morteza Mardani, Jiaming Song, Jan Kautz, and Arash Vahdat. A variational perspective on solving inverse problems with diffusion models. In *International Conference on Learning Representations (ICLR)*, 2024.

[37] Nick McGreivy and Ammar Hakim. Weak baselines and reporting biases lead to overoptimism in machine learning for fluid-related partial differential equations. *Nature Machine Intelligence*, 6(10):1256–1269, October 2024.

[38] Ben Mildenhall, Pratul P Srinivasan, Matthew Tancik, Jonathan T Barron, Ravi Ramamoorthi, and Ren Ng. Nerf: Representing scenes as neural radiance fields for view synthesis. *Communications of the ACM*, 65(1):99–106, 2021.

[39] Andrey Okhotin, Dmitry Molchanov, Arkhipkin Vladimir, Grigory Bartosh, Viktor Ohanesian, Aibek Alanov, and Dmitry P Vetrov. Star-shaped denoising diffusion probabilistic models. In *Advances in Neural Information Processing Systems 36 (NeurIPS)*, pages 10038–10067, 2023.

[40] Vivek Oommen, Aniruddha Bora, Zhen Zhang, and George Em Karniadakis. Integrating neural operators with diffusion models improves spectral representation in turbulence modeling. *arXiv preprint arXiv:2409.08477*, 2024.

[41] Xinyu Peng, Ziyang Zheng, Wenrui Dai, Nuoqian Xiao, Chenglin Li, Junni Zou, and Hongkai Xiong. Improving Diffusion Models for Inverse Problems Using Optimal Posterior Covariance. In *Proceedings of the International Conference on Machine Learning (ICML)*, 2024.

[42] Ben Poole, Ajay Jain, Jonathan T Barron, and Ben Mildenhall. DreamFusion: Text-to-3D using 2D diffusion. In *International Conference on Learning Representations (ICLR)*, 2023.

[43] Merle C. Potter and Bassem H. Ramadan. *An Introduction to Fluid Mechanics*. Springer Cham, 4 edition, 2012.

[44] Maziar Raissi, Paris Perdikaris, and George E. Karniadakis. Physics-informed neural networks: A deep learning framework for solving forward and inverse problems involving nonlinear partial differential equations. *Journal of Computational Physics*, 378:686–707, 2019.

[45] Pratik Rathore, Weimu Lei, Zachary Frangella, Lu Lu, and Madeleine Udell. Challenges in training PINNs: A loss landscape perspective. In *Proceedings of the 41st International Conference on Machine Learning (ICML)*, 2024.

[46] Shahed Rezaei, Ali Harandi, Ahmad Moeineddin, Bai-Xiang Xu, and Stefanie Reese. A mixed formulation for physics-informed neural networks as a potential solver for engineering problems in heterogeneous domains: Comparison with finite element method. *Computer Methods in Applied Mechanics and Engineering*, 401, 2022.

[47] Severi Rissanen, Markus Heinonen, and Arno Solin. Free hunch: Denoiser covariance estimation for diffusion models without extra costs. In *International Conference on Learning Representations (ICLR)*, 2025.

[48] Hermann Schlichting and Klaus Gersten. Onset of turbulence (stability theory). In *Boundary-Layer Theory*, chapter 15, pages 415–419. Springer, ninth edition, 2017.

[49] Aliaksandra Shysheya, Cristiana Diaconu, Federico Bergamin, Paris Perdikaris, José Miguel Hernández-Lobato, Richard Turner, and Emile Mathieu. On conditional diffusion models for pde simulations. *Advances in Neural Information Processing Systems*, 37:23246–23300, 2024.

[50] Jascha Sohl-Dickstein, Eric Weiss, Niru Maheswaranathan, and Surya Ganguli. Deep unsupervised learning using nonequilibrium thermodynamics. In *Proceedings of the 32nd International Conference on Machine Learning (ICML)*, volume 37 of *Proceedings of Machine Learning Research*, pages 2256–2265, Lille, France, 2015. PMLR.

[51] Jiaming Song, Arash Vahdat, Morteza Mardani, and Jan Kautz. Pseudoinverse-Guided Diffusion Models for Inverse Problems. In *International Conference on Learning Representations (ICLR)*, 2023.

[52] Jiaming Song, Qinsheng Zhang, Hongxu Yin, Morteza Mardani, Ming-Yu Liu, Jan Kautz, Yongxin Chen, and Arash Vahdat. Loss-guided diffusion models for plug-and-play controllable generation. In *Proceedings of the 40th International Conference on Machine Learning (ICML)*, volume 202 of *Proceedings of Machine Learning Research*, pages 32483–32498. PMLR, 2023.

[53] Yang Song, Jascha Sohl-Dickstein, Diederik P. Kingma, Abhishek Kumar, Stefano Ermon, and Ben Poole. Score-Based Generative Modeling through Stochastic Differential Equations. In *International Conference on Learning Representations (ICLR)*, 2021.

[54] Zhiwei Tang, Jiangweizhi Peng, Jiasheng Tang, Mingyi Hong, Fan Wang, and Tsung-Hui Chang. Tuning-free alignment of diffusion models with direct noise optimization. In *ICML 2024 Workshop on Structured Probabilistic Inference & Generative Modeling*, 2024.

[55] Jakub M. Tomczak. *Deep Generative Modeling*. Springer Cham, 1 edition, February 2022.

[56] Mario Lino Valencia, Tobias Pfaff, and Nils Thuerey. Learning distributions of complex fluid simulations with diffusion graph networks. In *The Thirteenth International Conference on Learning Representations*, 2025.

[57] Pascal Vincent. A connection between score matching and denoising autoencoders. *Neural Computation*, 23(7):1661–1674, 2011.

[58] Yinhuai Wang, Jiwen Yu, and Jian Zhang. Zero-shot image restoration using denoising diffusion null-space model. In *International Conference on Learning Representations (ICLR)*, 2023.

[59] Zhengyi Wang, Cheng Lu, Yikai Wang, Fan Bao, Chongxuan Li, Hang Su, and Jun Zhu. Prolificdreamer: High-fidelity and diverse text-to-3d generation with variational score distillation. In *Advances in Neural Information Processing Systems 36 (NeurIPS)*, pages 8406–8441, 2023.

[60] William W. Woessner and Eileen P. Poeter. Chapter 4: Darcy's law, head, gradient and hydraulic conductivity. In *Hydrogeologic Properties of Earth Materials and Principles of Groundwater Flow*. The Groundwater Project, Guelph, Ontario, Canada, 2020.

[61] Jiachen Yao, Abbas Mammadov, Julius Berner, Gavin Kerrigan, Jong Chul Ye, Kamyar Azizzadenesheli, and Anima Anandkumar. Guided diffusion sampling on function spaces with applications to pdes. *arXiv preprint arXiv:2505.17004*, 2025.

[62] Lvmin Zhang, Anyi Rao, and Maneesh Agrawala. Adding conditional control to text-to-image diffusion models. In *Proceedings of the IEEE/CVF international conference on computer vision*, pages 3836–3847, 2023.

[63] Yuanzhi Zhu, Kai Zhang, Jingyun Liang, Jiezhang Cao, Bihan Wen, Radu Timofte, and Luc Van Gool. Denoising diffusion models for plug-and-play image restoration. In *Proceedings of the IEEE/CVF Conference on Computer Vision and Pattern Recognition Workshops (CVPRW)*, pages 1219–1229, 2023.

[64] Zongren Zou, Xuhui Meng, and George Em Karniadakis. Correcting model misspecification in physics-informed neural networks (PINNs). *Journal of Computational Physics*, 505, 2024.

Appendices

A Proofs

Proposition 3.1. *Let $D^*_{reg}(x_t, t)$ be the denoiser that minimizes the regularized objective $\mathcal{L}_{reg}$. The optimal denoiser output is shifted from the true conditional mean of the data distribution by a term proportional to the gradient of the residual. Specifically:*

$$D^*_{reg}(x_t, t) = \mathbb{E}[x_0|x_t] - \lambda \left[\nabla_y \mathcal{R}(y)\right]^\top \mathcal{R}(y)\Big|_{y=D^*_{reg}}, \tag{11}$$

where we assume a scalar constraint residual for simplicity, or $\mathcal{R}$ represents the norm function directly. Since $\mathbb{E}[x_0 \mid x_t]$ does not generally satisfy the constraint, and the residual or its gradient are zero only when the constraint is satisfied, the optimal denoiser output is shifted. The asymptotic distributional guarantees of diffusion models are thus lost since there is no connection between the optimal denoiser and the score function $\nabla_{\boldsymbol{x}_t} \log p(\boldsymbol{x}_t)$.

Proof. Let $y = D_\theta(x_t, t)$. The objective can be rewritten as the expected risk for a given input x_t:

$$J(y) = \mathbb{E}_{x_0|x_t}\left[\|y - x_0\|^2\right] + \lambda\|\mathcal{R}(y)\|^2. \tag{14}$$

To find the optimum y^*, we take the gradient with respect to y and set it to zero:

$$\nabla_y J(y) = \nabla_y \left(\|y\|^2 - 2y^\top \mathbb{E}[x_0|x_t] + \mathbb{E}[\|x_0\|^2]\right) + \lambda\nabla_y\|\mathcal{R}(y)\|^2 \tag{15}$$

$$0 = 2(y - \mathbb{E}[x_0|x_t]) + 2\lambda(\nabla_y \mathcal{R}(y))^\top \mathcal{R}(y). \tag{16}$$

Solving for y yields the result. Consequently, $D^*_{\text{reg}}(x_t, t) \neq \mathbb{E}[x_0|x_t]$ unless $\lambda = 0$ or the constraint gradient is zero. □

Proposition 3.2. *The use of the regularized denoiser D^*_{reg} strictly increases the Evidence Lower Bound (ELBO) loss component compared to the vanilla denoiser $D^*_{vanilla}$. That is, the model's approximation of the data likelihood deteriorates.*

Proof. The standard diffusion loss $\mathcal{L}_{\text{diff}} = \mathbb{E}[\|D_\theta(x_t, t) - x_0\|^2]$ corresponds to the variational bound on the negative log-likelihood if using a specific weighting $w(t)$[31]. It is a well-known result that the unique global minimizer of this quadratic loss is the conditional expectation $D^*_{\text{vanilla}}(x_t, t) = \mathbb{E}[x_0|x_t]$.

Since $D^*_{\text{reg}}(x_t, t) \neq \mathbb{E}[x_0|x_t]$ (from Proposition 3.1), and $\mathcal{L}_{\text{diff}}$ is strictly convex with respect to the prediction y, it follows that:

$$\mathbb{E}_{x_0|x_t}\left[\|D^*_{\text{reg}}(x_t) - x_0\|^2\right] > \mathbb{E}_{x_0|x_t}\left[\|D^*_{\text{vanilla}}(x_t) - x_0\|^2\right]. \tag{17}$$

Specifically, by the bias-variance decomposition, the increase in the diffusion loss is exactly the squared magnitude of the shift derived in Proposition 3.1:

$$\Delta\mathcal{L} = \|D^*_{\text{reg}}(x_t, t) - \mathbb{E}[x_0|x_t]\|^2. \tag{18}$$

Thus, optimizing the regularized objective $\mathcal{L}_{\text{target}}$ forces the model to trade off data likelihood for constraint satisfaction, confirming the distributional bias observed in Table 1. □

B Additional Related Work

Inference Time Adjustment for Inverse Problems Many methods target adjusting diffusion models at inference time to solve inverse problems, many of them formally targeting approximation of Eq. (4). Song et al. [53] was one of earliest papers to propose inference-time adjustments to the diffusion model to solve problems like inpainting and color restoration. Chung et al. [10], Wang et al. [58], Zhu et al. [63] propose more advanced methods for a wider range of inverse problems. The first methods to make the explicit connection to Eq. (4) were [21, 11, 51]. While the method by Song et al. [51] only worked for linear inverse problems, Song et al. [52] generalized it to general guidance functions through Monte Carlo integration of Eq. (4). Works focused on improving the $p(\boldsymbol{x}_0 \mid \boldsymbol{x}_t)$ approximation include [4, 41, 47].

Hard-Constraint Diffusion via Modified Dynamics Several works impose constraints by *changing the diffusion dynamics* so that the support is restricted by construction. Riemannian diffusion models and flow matching models move the noising and denoising processes to a target manifold, enabling sampling on spheres, tori, hyperboloids, and matrix groups but requiring smooth geometry and geometric operators [13, 23, 6]. Fishman et al. [17, 18], Lou and Ermon [35] propose to use noising processes that are constrained within convex sets defined by inequality constraints. while [33] tackle the problem by learning standard diffusion models in a dual space created using a mirror map. *Star-shaped DDPMs* tailor noise to exponential-family distributions suited to constrained manifolds [39]. These methods provide hard constraints but are typically specialized to particular geometries or constraint classes.

Optimizing Samples to Match with Constraints Ben-Hamu et al. [3] generate samples with constraints by optimizing a source point in the noisy latent space such that the generative ODE solution matches with the constraint. Tang et al. [54] instead optimize the noise injected during the stochastic sampling process. Poole et al. [42] generate samples by directly optimizing the target image within a constrained space (e.g., images parameterized by a neural radiance field [38]), while minimizing the diffusion loss for the image. Wang et al. [59] extends the method with a particle-based variational framework. In a similar manner, Mardani et al. [36] formulate the sampling process as a optimizing a variational inference distribution on the clean samples.

C Darcy Flow

Darcy Flow refers to a set of equations used to study the (laminar) flow of fluids in porous media. In two dimensions it is defined by the following set of equations for $\boldsymbol{x} = (x, y)$ [48, 25, 2]:

$$\boldsymbol{u}(\boldsymbol{x}) = -K(\boldsymbol{x})\nabla p(\boldsymbol{x}) \tag{19}$$

$$\nabla \cdot \boldsymbol{u} = f(\boldsymbol{x}) \tag{20}$$

$$\boldsymbol{u} \cdot \hat{\boldsymbol{n}} = 0, \text{ boundary condition} \tag{21}$$

$$\int p(\boldsymbol{x})\, \mathrm{d}\boldsymbol{x} = 0, \tag{22}$$

where K is a permeability field that describes how easy a fluid flows through the medium, p is the pressure field that defines where the fluid is pushed and pulled, $\boldsymbol{u}$ the velocity field of the fluid (as visualized in Fig. 4) and f is the net flow of fluid through a given point. *Net* flow means that if there is the same amount fluid entering and exiting at a given point, then the net flow is zero. As a more concrete example, we can use Darcy flow to describe how water will flow through a body of sand. We can expect more water to flow at the areas where we apply more pressure to squeeze out the water.

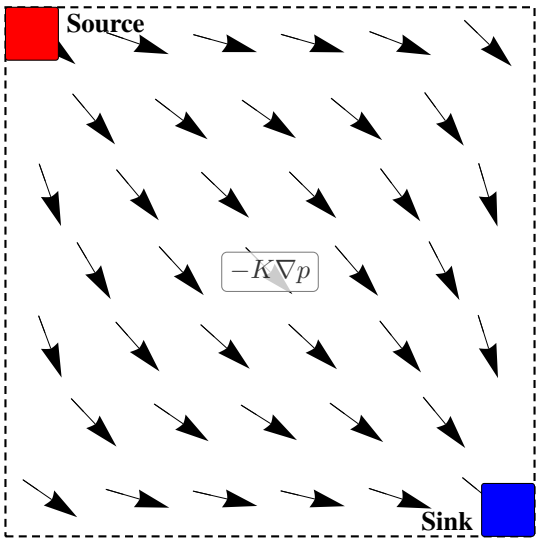

Figure 4: A simplified visual representation of the Darcy velocity field defined by $K\nabla p$.

There are many important assumptions around Darcy flow before it is applicable. We must have laminar flow at steady state, which means that there must not be sudden changes in the flow of the fluid. This depends on the geometry of the body that the fluid is traversing through, its viscosity, its speed, among other factors that are generally described through the Reynolds number Schlichting and Gersten [48], Potter and Ramadan [43]. The Reynolds number needed to break into critical flow also will change between different configurations, so it may be difficult to know a priori if Darcy flow is an appropriate way to model the system.

Through experience it has been observed that the Darcy flow approximation can work well for media that are "fine-grained" enough, as the gaps between the particles in the porous matrix do not break the flow of water Woessner and Poeter [60]. However, at a big enough particle size, water starts to bounce more between collisions, causing the flow to become more turbulent.

C.1 Qualitative results from Darcy Flow

Fig. 5 shows a histogram of the learned distribution of values for pressure and permeability using each of the compared methods. Particularly, as noted by [2], PIDM presents excessive bias compared to the other methods.

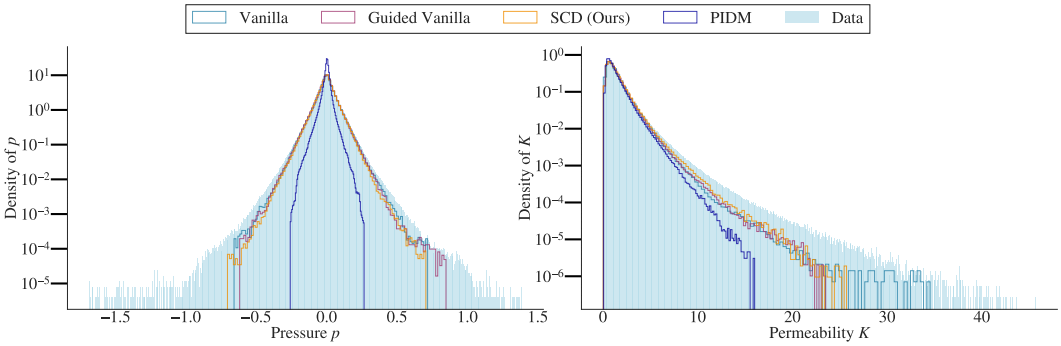

Figure 5: Darcy flow validation. 1000 samples were generated with each approach, using 100 denoising steps for each. Error bars indicate the minimum and maximum from the samples. The distribution PIDM learns is highly biased; all other methods have higher distributional fidelity. Particularly, our method shows low distributional bias compared to vanilla.

Qualitative samples using each of the methods can be seen in Fig. 6.

D Additional Results from the Helmholtz Equation

The Helmholtz Differential Equation is used to model the propagation of waves through (possibly heterogeneous) media. Its 2-dimensional version is given by:

$$\mathcal{R}_{\text{Helmholtz}}(u, a) = \nabla^2 u(\boldsymbol{x}) + k^2 u(\boldsymbol{x}) - a(\boldsymbol{x}) = 0, \quad \boldsymbol{x} \in (0, 1)^2, \tag{23}$$

where u is known as the solution field, a the source field and k the wave number. With this presentation, the solution is given by a spatial wave in 2 dimensions and boundary conditions equal to 0. This equation is particularly important in acoustics and electromagnetics, describing the way sound and light travel through space. It is generally subject to the measurement of k, which uniquely defines the solution of the system given the boundary conditions. The wave number is usually estimated with sensor readings in noisy media, which subjects the equation to observation error.

Similar to our approach to Darcy Flow, we use Eq. (23) as the residual to define $r_c = \exp(-\left|\mathcal{R}_{\text{Helmholtz}(u,a)}\right|)$, where u and a correspond to the denoiser outputs. Following Yao et al. [61], we use a discretization of u and a in $\mathbb{R}^{128\times128}$ modeled by the Diffusion Model with the same UNet backbone as Darcy and a wave number $k = 1$. The training details are available in Appendix F.4.

Distributional Fidelity, Misspecification and Residuals In this setting, we induce the misspecifications through the addition of Gaussian noise to the wave number. The degree of misspecification is handled by the standard deviation of this noise, and this experiment allows us to measure how sensitive SCD can be to noisy gradients through the constraint function. The results are summarized

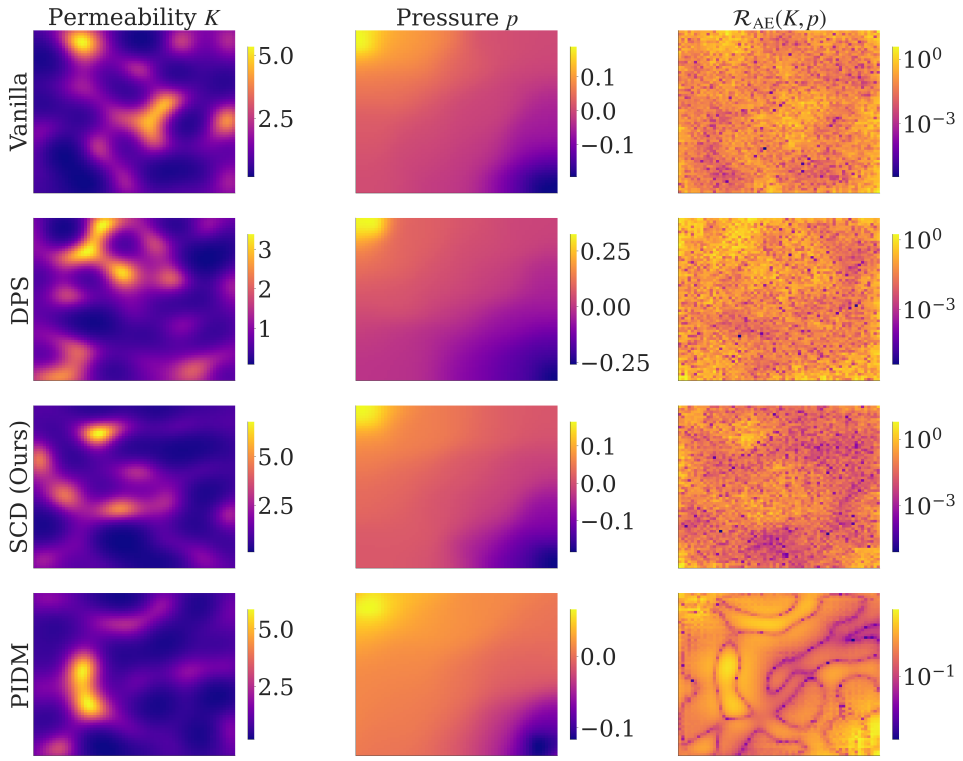

Figure 6: Residuals and samples produced by vanilla diffusion, DPS guidance, SCD and PIDM.

Table 3: Measured (**best**, second best) residual values and validation set NLL of the different methods across different levels of source and sink misspecification. Our method shows good performance across all misspecification levels. Residual values presented are mean absolute residuals across 1000 samples with two standard deviations and NLL values are on the complete validation set, reported in bits/dim. Vanilla does not use the constraint knowledge, so we treat it the same for all levels as a baseline. Lower is better.

		Original	*increasing misspecificication* →		
Metric	**Method**	$\sigma_{\text{obs}} = 0$	$\sigma_{\text{obs}} = 0.05$	$\sigma_{\text{obs}} = 0.1$	$\sigma_{\text{obs}} = 0.5$
Residual	Vanilla	0.035 ± 0.007	0.035 ± 0.007	0.035 ± 0.007	0.035 ± 0.007
	FunDPS	13.84 ± 3.4	13.86 ± 3.4	13.84 ± 3.3	14.2 ± 3.4
	DPS	0.032 ± 0.004	0.033 ± 0.005	0.035 ± 0.004	0.034 ± 0.003
	SCD (ours)	$\mathbf{0.025 \pm 0.003}$	$\mathbf{0.024 \pm 0.003}$	$\mathbf{0.024 \pm 0.002}$	$\mathbf{0.023 \pm 0.003}$
NLL	Vanilla	$\mathbf{-21.6}$	$\mathbf{-21.6}$	$\mathbf{-21.6}$	$\mathbf{-21.6}$
	FunDPS	-7.2	-7.3	-7.2	-7.2
	DPS	$\mathbf{-21.6}$	-21.5	-21.5	-21.5
	SCD (ours)	$\mathbf{-21.6}$	-21.5	-21.5	-21.5

in Table 3, where we compare our results with the guidance framework FunDPS using a model trained by the authors [61], a vanilla diffusion model and DPS guidance on the vanilla diffusion model. The FunDPS sampling is done with a combination of a reconstruction loss based on partial observations and the residual to observe the issues resulting from imbalanced guidance. SCD manages to preserve the NLL with the most competitive residual values in this task. It is evident that using this combined guidance in FunDPS heavily favors the reconstruction error, essentially forfeiting the physical consistency of the generated samples. On the other hand, regular DPS only sees marginal improvements in terms of the residuals compared to the vanilla diffusion model.

E Loss-Guided Diffusion Models

Loss-Guided Diffusion Models were proposed by Song et al. [52] as a "plug-and-play" guidance method to make pre-trained diffusion models generate better constraint-compliant samples at inference time. The core idea is that a learned unconditional score $s_\theta^* \approx \nabla_{\boldsymbol{x}_t} \log p(\boldsymbol{x}_t)$ acts as a prior to which we can apply Bayes' rule for a posterior $p(\boldsymbol{x}_t|c)$ with some condition c:

$$\nabla_{\boldsymbol{x}_t} \log p\left(\boldsymbol{x}_t|c\right) = \nabla_{\boldsymbol{x}_t} \log \left(\frac{p\left(c|\boldsymbol{x}_t\right) p\left(\boldsymbol{x}_t\right)}{p(c)} \right) \tag{24}$$

$$= \nabla_{\boldsymbol{x}_t} \log p\left(c|\boldsymbol{x}_t\right) + \nabla_{\boldsymbol{x}_t} \log p\left(\boldsymbol{x}_t\right) - \cancelto{0}{\nabla_{\boldsymbol{x}_t} \log p(c)} \tag{25}$$

$$= \nabla_{\boldsymbol{x}_t} \log p\left(c|\boldsymbol{x}_t\right) + \nabla_{\boldsymbol{x}_t} \log p\left(\boldsymbol{x}_t\right), \tag{26}$$

where $\boldsymbol{x}_t$ is the diffusion sample at time t and c is a condition for the generative process, and we have used the fact that $\log p(c)$ is a constant so its gradient is 0. The likelihood term $p(c|\boldsymbol{x}_t)$ is analytically untractable, as the condition c only applies to clean samples $\boldsymbol{x}_0$. However, we can write it as follows:

$$p(c|\boldsymbol{x}_t) = \int_{\boldsymbol{x}_0} p(c|\boldsymbol{x}_0, \boldsymbol{x}_t) p(\boldsymbol{x}_0|\boldsymbol{x}_t) \mathrm{d}\boldsymbol{x}_0 = \int_{\boldsymbol{x}_0} p(c|\boldsymbol{x}_0) p(\boldsymbol{x}_0|\boldsymbol{x}_t) \mathrm{d}\boldsymbol{x}_0, \tag{27}$$

where we have assumed that c is conditionally independent of $\boldsymbol{x}_t$ when given $\boldsymbol{x}_0$. We then take the approximation:

$$p(\boldsymbol{x}_0|\boldsymbol{x}_t) \approx \mathcal{N}\left(\boldsymbol{x}_0|\mu, \Sigma\right), \tag{28}$$

with mean parameter μ and covariance parameter Σ, as this allows us to use Tweedie's formula, connecting the score function with the exact moments of $p(\boldsymbol{x}_0|\boldsymbol{x}_t)$ [15, 47]:

$$\mu = \mathbb{E}[\boldsymbol{x}_0|\boldsymbol{x}_t] = \boldsymbol{x}_t + \sigma_t^2 \nabla_{\boldsymbol{x}_t} \log p(\boldsymbol{x}_t) \tag{29}$$

$$\Sigma = \mathbb{C}\mathrm{ov}[\boldsymbol{x}_0|\boldsymbol{x}_t] = \sigma_t^2 \left(\sigma_t^2 \underbrace{\nabla_{\boldsymbol{x}_t}^2 \log p(\boldsymbol{x}_t)}_{\text{Hessian}} + \mathbf{I} \right). \tag{30}$$

Since the Hessian is expensive to evaluate in high-dimensional data, it is common to see the approximation $\Sigma \approx \sigma_{0|t}^2 \mathbf{I}$ be used, and this is the choice taken by Song et al. [52]. Then, we can assume that the likelihood on clean samples $p(c|\boldsymbol{x}_0)$ can be expressed with a differentiable, lower-bounded constraint loss function $\ell_c : \mathcal{X}_0 \to \mathbb{R}$ by:

$$p(c|\boldsymbol{x}_0) = \frac{\exp\left(-\ell_c(\boldsymbol{x}_0)\right)}{Z}, \tag{31}$$

where $Z = \int_{\boldsymbol{x}_0} p(\boldsymbol{x}_0) \exp\left(-\ell_c(\boldsymbol{x}_0)\right) \mathrm{d}\boldsymbol{x}_0$ is a normalizing constant. Plugging equation 31 into equation 24, we get:

$$\nabla_{\boldsymbol{x}_t} \log p\left(\boldsymbol{x}_t|c\right) = \nabla_{\boldsymbol{x}_t} \log p\left(\boldsymbol{x}_t\right) + \nabla_{\boldsymbol{x}_t} \log \int_{\boldsymbol{x}_0} \exp\left(-\ell_c(\boldsymbol{x}_0)\right) \mathcal{N}\left(\boldsymbol{x}_0; \mu, \sigma_{0|t}^2 \mathbf{I}\right) \mathrm{d}\boldsymbol{x}_0. \tag{32}$$

Song et al. [52] point out that Chung et al. [11]'s DPS is a special case of this equation taking $\sigma_{0|t} \to 0$ and with ℓ_c being a linear projection. Song et al. [52] then proposes the approximation to the integral by using Monte Carlo integration with $\sigma_{0|t}^2 = \frac{\sigma_t^2}{1+\sigma_t{}^2}$. We adopt this scheme with 16 Monte Carlo samples to guide the vanilla diffusion model for our Darcy Flow experiments as a baseline.

F Architectures and training details

The architectures and experiments on this work were implemented using PyTorch 2.4.1. All experiments were ran on single GPUs, from either NVIDIA H200, H100, A100 or V100 GPUs. For both experiments, γ_θ is implemented as a 2-layer MLP with an embedding dimension of 100. The input for either task is the denoiser output $D_\theta(\boldsymbol{x_t}, t)$ and the diffusion time t. Between each layer there is an ELU activation function to ensure that the scaling factor remains positive.

F.1 Modified Loss Function

The loss function by Karras et al. [27] has the form seen in Eq. (3) with the choice of distributions $t \sim \text{LogNormal}(\mu_{\text{train}}, \sigma^2_{\text{train}})$ and $\boldsymbol{x}_t \sim \mathcal{N}(\boldsymbol{x}_0, t\mathbf{I})$, and weighting function $w(t) = (t + \sigma_{\text{data}^2})/(t\sigma^2_{\text{data}})$. Crucially, the choice for the distribution for t is free, i.e. a design choice; Karras et al. [27] choose the log-normal distribution based on the observation that most of the important denoising steps in a diffusion model happen in the "intermediate" noise levels, since at high noise levels there is little distinction between steps and at very-low noise levels the differences are negligible. However, on the ODE problems presented in this paper we have observed that low noise levels have a substantial effect on the final residuals. Simply trying to set μ_{train} to a small value can cause numerical stability issues, because it may start sampling values that are too small and consequently make the weighting function blow up.

Following this, and based on the observation that in practice most numerical integration samplers always end at a predetermined minimum time step, we choose the noise level distribution $t \sim \text{TruncLogNormal}(\mu_{\text{train}}, \sigma^2_{\text{train}}, a)$ where a defines the lowest possible noise level to be sampled. With this change, we noticed a substantial improvement in the residuals in the Darcy Flow experiment, with the results shown in Table 4. We use a mean of -1.5 and standard deviation of 1.2 for the log-normal loss and a mean of -2, standard deviation of 1.7 and truncation lower limit of -4 for the truncated log-normal loss.

Table 4: Residuals obtained in the Darcy flow experiments using the noise level distribution $t \sim \text{LogNormal}(\mu_{\text{train}}, \sigma^2_{\text{train}})$ by Karras et al. [27] and our choice $t \sim \text{TruncLogNormal}(\mu_{\text{train}}, \sigma^2_{\text{train}}, a)$. Using the truncated log-normal shows a substantial improvement over the log-normal in this task.

		Original	*increasing misspecificication* →		
Distribution	**Method**	$f_{\max} = 10$	$f_{\max} = 20$	$f_{\max} = 30$	$f_{\max} = 40$
log-normal	Vanilla	0.874 ± 0.411	0.874 ± 0.411	0.874 ± 0.411	0.874 ± 0.411
	Guided Vanilla	0.869 ± 0.382	0.862 ± 0.372	0.872 ± 0.404	0.869 ± 0.379
	SCD (ours)	0.342 ± 0.136	0.414 ± 0.174	0.429 ± 0.173	0.428 ± 0.174
Truncated log-normal	Vanilla	0.157 ± 0.071	0.157 ± 0.071	0.157 ± 0.071	0.157 ± 0.071
	Guided Vanilla	0.141 ± 0.063	0.139 ± 0.067	0.140 ± 0.065	0.139 ± 0.066
	SCD (ours)	0.113 ± 0.048	0.106 ± 0.049	0.114 ± 0.059	0.118 ± 0.051

Following these results, we use the truncated log-normal distribution for all our experiments.

F.2 Circles

For the toy example we use a 3 layer MLP with an embedding dimension of 128. To train the networks we use the Adam optimizer with $\beta_1 = 0.9$, $\beta_2 = 0.999$ and a fixed learning rate of $\alpha = 1 \cdot 10^{-4}$.

The data set consisted of 10000 points sampled from the unit circle, and the models were trained over 1000 epochs with a batch size of 128.

For the "Dent" variant of misspecification, we use the following parametric curve:

$$C(\theta) = (r(\theta)\cos(\theta), r(\theta)\sin(\theta)) \tag{33}$$

$$r(\theta) = 1 - 0.25 \cdot \beta\left(\frac{\text{wrap}(\theta - \frac{\pi}{2})}{1.2}, 5\right) \cdot \left(1 + 0.6\left(1 - 2\left(\frac{\text{wrap}(\theta - \frac{\pi}{2})}{1.2}\right)^2\right)\right) \tag{34}$$

$$\text{wrap}(\theta) = ((\theta + \pi) \mod 2\pi) - \pi \tag{35}$$

$$\beta(u, 5) = \begin{cases} (1 - u^2)^5 : |u| < 1 \\ 0 \text{ otherwise,} \end{cases} \tag{36}$$

where C defines the coordinates of every point in the curve in polar coordinatese.

F.3 Darcy Flow

For Darcy Flow we used the UNet implementation by Karras et al. [28]. We use the Heun sampler implementation by Karras et al. [27] with 100 denoising steps. The used hyperparameters on the network are summarized on Table 5.

Table 5: Architecture hyperparameters for the Darcy Flow experiments

Hyperparameter	Value
Model channels	24
Number of residual blocks	8
Per-resolution multipliers	[1, 2, 3, 4]
Attention resolutions	[16, 8]

F.4 Helmholtz Equation

For the Helmholtz Equation we used the UNet implementation by Karras et al. [28]. We use the Heun sampler implementation by Karras et al. [27] with 100 denoising steps. The used hyperparameters on the network are summarized on Table 6.

Table 6: Architecture hyperparameters for the Helmholtz Equation experiments

Hyperparameter	Value
Model channels	32
Number of residual blocks	8
Per-resolution multipliers	[1, 2, 3, 4]
Attention resolutions	[16, 8]

F.5 Runtimes

The details on the runtimes on an NVIDIA H200 GPU with vanilla diffusion and our method are shown in Table 7. We note that our method sees the most impact at sampling time, since the overhead duplicates per each sampling iteration because the Heun sampler makes two neural function evaluations per iteration.

Table 7: Runtimes of vanilla and our method on training and sampling on an NVIDIA H200 GPU. Sampling is done for eight samples at a time using the Heun sampler implementation by Karras et al. [27]. Numbers are reported as a mean with two standard errors over 300 iterations. Units of time are specified for each column.

Method	**Training iteration wall clock time (ms)**	**Sampling iteration wall clock time (s)**
Vanilla	110 ± 3.62	7.79 ± 0.021
SCD (ours)	148 ± 2.25	10.3 ± 0.029

The baseline PIDM results were reproduced with a pre-trained model provided by Bastek et al. [2], and for the misspecification experiments we trained a diffusion model with PIDM with each misspecified residual using the same hyperparameter setups as Bastek et al. [2]. The vanilla score-matching and SCD networks were trained using Adam with an initial learning rate of $2 \cdot 10^{-3}$ and weight decay as detailed by Karras et al. [28]. Both the vanilla model and SCD were trained for 300k iterations, although SCD plateaus at around 250k. We use a batch size of 64. For all experiments we use Exponentially Moving Averages for sample generation with a decay rate of 0.99.

G Additional “chop” samples

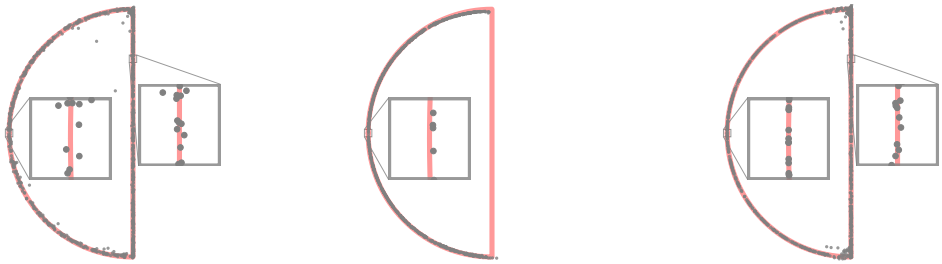

(a) Vanilla diffusion (b) PIDM (baseline) (c) SCD (ours)

Figure 7: Additional samples from the “chop” example.